Yielding and bifurcated aging in nanofibrillar networks

Ryan Poling-Skutvik [1] Eoin McEvoy,[2,3] Vivek Shenoy,[2,3] and Chinedum O. Osuji[1,*]

[1]*Department of Chemical and Biomolecular Engineering, University of Pennsylvania, Philadelphia, Pennsylvania 19104, USA*
[2]*Center for Engineering Mechanobiology, University of Pennsylvania, Philadelphia, Pennsylvania 19104, USA*
[3]*Department of Materials Science and Engineering, University of Pennsylvania, Philadelphia, Pennsylvania 19104, USA*

Although phenomenologically simple to define, the yield stress is often difficult to quantify unambiguously in practice, especially for thixotropic materials with complex shear histories. Here, we identify a stress-controlled bifurcation in the yielding response of cellulose nanofibril gels, which we show can rigorously localize the yield stress in disordered materials with time-dependent behavior. After an initial yielding event, the fibrillar networks subsequently yield faster and at lower magnitudes of stress. For low stresses, the time to yielding increases with waiting time t_w and diverges once the network has restored sufficient entanglement density to support the stress. For higher stresses, the yield time instead plateaus at a finite value because the developed network density is insufficient to support the applied stress. We quantitatively relate the yielding and aging behavior of the network to the competition between stress-induced disentanglement and dynamic fluctuations of the fibrils rebuilding the network. The critical stress σ_c that bifurcates the response of the material between these two states identifies the intrinsic yield stress in these disordered materials, independent of aging, thixotropic effects, or shear history.

How materials transition from an elastic solid to flowing as a viscous liquid (i.e., the yield transition) has been investigated for over a century but the physical underpinnings continue to be debated. Many investigations relate the yield transition to a specific yield stress σ_y or yield strain γ_y that causes the material to deviate from linear elasticity by displaying unrecoverable strain. Although yielding is phenomenologically simple to comprehend, the quantities σ_y and γ_y are often defined empirically and arbitrarily [1–3]. Even for standard yield stress fluids, these quantities can vary by an order of magnitude depending on the measurement technique and choice of definition [4], making comparisons across studies or between materials difficult.

Characterizing the yield transition becomes even more challenging for thixotropic materials or fluids that strongly age because shear history significantly affects flow behavior [5–7]. In thixotropic materials, flow curves often exhibit strong hysteresis with different apparent yield stresses when subjected to increasing or decreasing shear rates [8]. More careful characterizations measure the evolution of viscosity over time as thixotropic materials are sheared and observe that the viscosity bifurcates across a critical shear stress that separates a fluidlike state from a solidlike state [9]. In this manner, the stress that controls the viscosity bifurcation can be interpreted as the single yield stress of the material. This critical stress, however, is measured under flow and therefore couples to the competition between the kinetics with which the fluid builds structure and the imposed rate of shear [10]. Indeed, viscosity bifurcation occurs at a significantly higher stress if the material is allowed to age in the absence of shear

for even a short period of time before being subjected to shear [9,10]. Thus, there remains a critical need to precisely localize the yield stress of thixotropic materials in a manner that is independent of shear history or sample age.

In this Rapid Communication, we exploit a bifurcation in the yielding response of a thixotropic network of cellulose nanofibrils (CNF) to identify a unique critical stress σ_c that controls the yielding transition. Because the CNF gels are formed through physical entanglements, yielding results in the local destruction of the network and allows the gels to subsequently yield at much lower stresses. We map the change in yield time t_y as a function of the waiting time t_w between yielding events at different σ and observe a bifurcation in which t_y diverges at low stress (i.e., the material behaves like a solid) but plateaus for high stress (i.e., the material behaves like a fluid). At the critical stress σ_c, t_y evolves as a power law with respect to t_w. In contrast to viscosity bifurcation, σ_c does not depend on the shear history imposed on the material or the sample age and thus represents a unique and unambiguous measurement of the material yield stress σ_y. We then use standard models of entanglement-controlled dynamics and stress-activated bond rupture to demonstrate that the evolution of the yielding kinetics arises from the nanoscale fibril dynamics. From these findings, we develop a comprehensive physical picture describing the behavior of soft, amorphous materials across the yielding transition.

A stock suspension of TEMPO-modified cellulose nanofibrils (CNF) was acquired from the Process Development Center at the University of Maine at a concentration of 1.1 wt.% and a surface charge concentration of 1.5 mM per gram of dry CNF. The stock solution was diluted by mixing with deionized water and bath sonicating for 10 min or concentrated using a rotary evaporator. All samples were
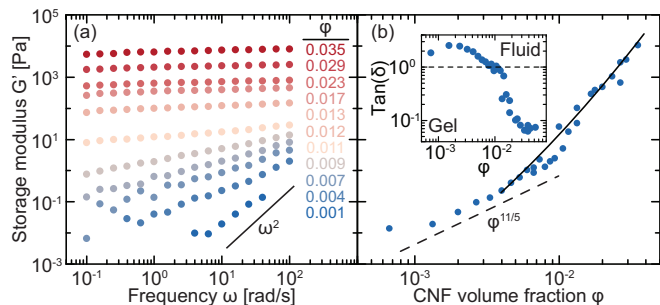
FIG. 1. Storage modulus G' for fibrillar suspensions as a function of (a) frequency at various concentrations and (b) concentration at $\omega = 10 \text{ rad s}^{-1}$. Dashed curve represents predicted scaling for suspensions of semiflexible fibers [13] and solid curve indicates predictions for fibrillar networks [16]. *Inset*: Ratio of moduli $\tan(\delta) \equiv G''/G'$ at $\omega = 10 \text{ rad s}^{-1}$.

visually uniform and transparent, indicating that the CNF remained homogeneously suspended. Volume fractions ϕ are estimated from weight fractions assuming the specific gravity of cellulose nanofibrils $s = 1.5$. Oscillatory and steady shear rheological measurements were performed on a strain-controlled ARES G2 with a 25 mm cone geometry with an angle of 0.1 rad. Creep measurements were performed on a stress-controlled Anton-Paar MCR301 rheometer with a 50 mm parallel plate geometry and a gap size of 1 mm. Sample edges were coated with a thin layer of light mineral oil to prevent evaporation. During the creep experiments, samples are yielded by either applying a constant stress $\approx 2\sigma_c$ or under a constant shear rate $\dot{\gamma} = 1 \text{ rad s}^{-1}$ until the sample reaches a strain between 500 and 1000%. After this yielding protocol, the sample is allowed to rest under zero external stress for a waiting time t_w after which a stress σ is imposed and the sample compliance is measured.

Before investigating how these fibrillar suspensions yield, we characterize their static mechanical properties and show that they are strongly dependent on the suspension volume fraction ϕ (Fig. 1). The rheology of the suspensions originates due to physical interactions akin to entanglements and to weak association involving Van der Waals interactions and hydrogen bonding [11,12]. When $\phi \lesssim 0.01$, the CNF form viscoelastic fluids in which the storage modulus scales as $G' \sim \phi^{11/5}$ in good agreement with predictions for suspensions of semiflexible fibers that account for stretching entropy and fibrillar bending rigidity [13]. At higher concentrations, the suspensions form viscoelastic gels (i.e., $\tan(\delta) < 1$) in which G' increases more rapidly, indicating that $\phi \approx 0.01$ serves as the phenomenological gel point of the system. The rapid increase in G' with ϕ is consistent with previous investigations [14,15] and with a recent model in which elastic energy is stored in deflections of simply supported beams [16]. Additionally, the fact that G' is nearly independent of ω at high ϕ indicates that terminal relaxations of the network are suppressed.

We demonstrate the yielding characteristics of these fibrillar networks under stress by measuring the compliance of the gels as a function of time [Fig. 2(a)]. When subjected to low stresses, the CNF networks exhibit finite compliances
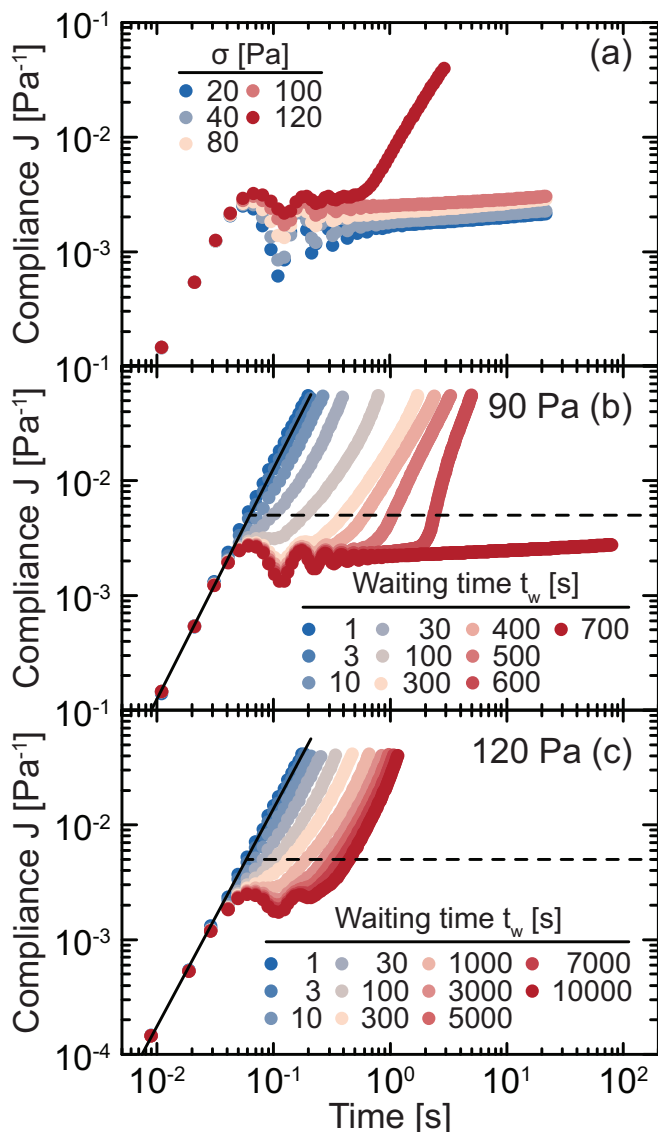

FIG. 2. (a) Compliance $J = \gamma/\sigma$ as a function of time for a fully equilibrated $\phi = 0.023$ fibrillar network under different stresses. Compliance J of the network after an initial yielding event with applied stress of (b) 90 Pa and (c) 120 Pa at various waiting times t_w. Solid lines indicate inertial response of instrument. Dashed lines indicate yielding thresholds.

after creep ringing, indicating that the gels behave like elastic solids that do not flow. Under large external stresses, however, the compliance initially plateaus on short time scales before increasing abruptly at a yield time t_y as the network begins to flow. Although the lowest value of stress that causes this upturn in compliance is often called the yield stress σ_y [2], the CNF gels exhibit a strongly thixotropic response and will yield readily upon subsequent applications of stress even if $\sigma \ll \sigma_y$. Thus, yielding depends strongly on the sample shear history and cannot be simply defined based on a single compliance curve (Fig. 2). Instead, we measure the compliance of gels after an initial yielding event as a function of σ and waiting time t_w. For small stresses (e.g., $\sigma = 90$ Pa for $\phi = 0.023$), t_y increases with increasing t_w until the sample
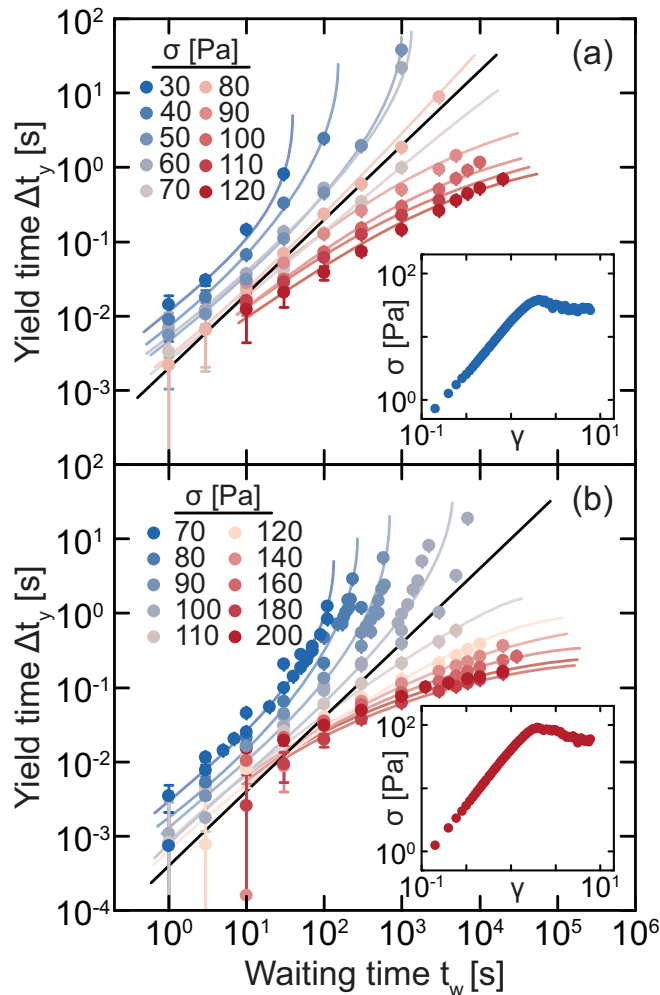
FIG. 3. Yield time Δt_y as a function of waiting time t_w under different applied stresses for fibrillar suspensions with (a) $\phi = 0.018$ and (b) $\phi = 0.023$. Colored curves are guides to the eye. Black curves illustrate critical bifurcation behavior. Insets: Stress σ as a function of strain γ measured at a constant shear rate of $\dot{\gamma} = 10^{-3}$ rad s^{-1}.

no longer yields and instead exhibits a finite compliance at long times. Physically, this finite compliance indicates that the CNF network has undergone kinetic restructuring to rebuild a dense enough entanglement network to support the applied stress without large-scale flow. By contrast, the CNF network always yields under high applied stresses (e.g., $\sigma = 120$ Pa for $\phi = 0.023$) even as t_y moderately increases over many decades of t_w.

We quantify the temporal shift in the compliance curves by defining the yield time Δt_y as the difference between the instrument's inertial response and the time when $J = 2J^*$ (dashed lines in Fig. 2), where J^* is the height of the first creep ringing peak. This definition unambiguously distinguishes between the yielding flow of the fibrillar network and the creep ringing of the instrument, which is especially important when considering yielding at low t_w. For all samples and all applied stresses, Δt_y increases with t_w but depends strongly on volume fraction and applied stress (Fig. 3). The increase in

Δt_y with increasing t_w indicates that the material dynamically changes under quiescent conditions, but because $t_w \gg \Delta t_y$, the CNF networks are at quasisteady state during each creep experiment. There is a distinct bifurcation in the behavior of Δt_y across the critical stress σ_c. For $\sigma < \sigma_c$, Δt_y increases convexly with t_w until it diverges, at which point the sample supports the applied stress without bulk flow. As σ increases, the divergence of the yield time curve occurs at larger t_w, indicating that it takes longer for the CNF network to dynamically restructure enough to accommodate the larger stress. By contrast, Δt_y increases concavely with t_w when $\sigma > \sigma_c$ to reach a plateau. The magnitude of this plateau decreases with increasing σ, indicating that higher stresses yield the networks more quickly. Separating the liquidlike response from the solidlike response of the network, the critical stress σ_c serves to define the yield transition in an analogous manner to the Winter-Chambon criterion defining the gel transition [17,18].

Although the yield transition is distinctly characterized from these compliance measurements, we can gain further insights into the mechanisms underlying this yielding event and resulting thixotropy of the material. Based on the creep experiments and the bifurcated aging response, we expect that the fibrillar networks yield by concentrating stress into a shear band [19,20], similar to the behavior of networks of associative polymers [21,22] and microgel suspensions [23]. The boundary of the shear bands represents a local minimum in entanglement density that allows the sample to flow. If the network is allowed to rest after yielding, individual fibers dynamically rebuild the entanglement network across the boundary to restore the physical properties of the bulk sample. This picture is reminiscent of the welding of two polymer melts [24,25]. The kinetics of this welding behavior is modeled by chains transporting across an interface through repetitive modes so that the planar chain density ρ follows

$$\frac{\rho(t)}{\rho_\infty} = \frac{2}{\sqrt{\pi}}\left(\tau^{1/2} + 2\sum_{k=1}^{\infty}(-1)^k \right.$$
$$\left. \times\, [\tau^{1/2}\exp(-k^2/\tau) - \sqrt{\pi}k\,\mathrm{erfc}(k/\tau^{1/2})]\right),$$
(1)

where $\tau = 2t_w/\tau_0 N^2$, τ_0 is a time scale related to the diffusion of a segment, N is the number of segments per chain, and ρ_∞ is the chain density at equilibrium [24]. Because the mechanical modulus of the network does not significantly change across repeated yieldings, we expect that CNF disentangle under flow rather than undergo scission. Creating an interface within the CNF network via disentanglement requires individual chains to be pulled out of the network. Each chain experiences a frictional drag ζ as it is pulled out so that the energy required to create an interface can be expressed as $G_c \sim \zeta \rho$ [26,27]. Using Griffith's fracture criteria [28], fracture energy is related to fracture stress according to $G_c = \pi a \sigma_c^2/E$, where a is related to the initial size of the fracture and E is the Young's modulus of the network. Combining these expressions leads to $\sigma(t)/\sigma_c \sim (\rho(t)/\rho_\infty)^{1/2}$, which accurately fits the restructuring kinetics of the CNF networks across many orders of magnitude in time and an order of magnitude in network strength (Fig. 4) with only one floating parameter,
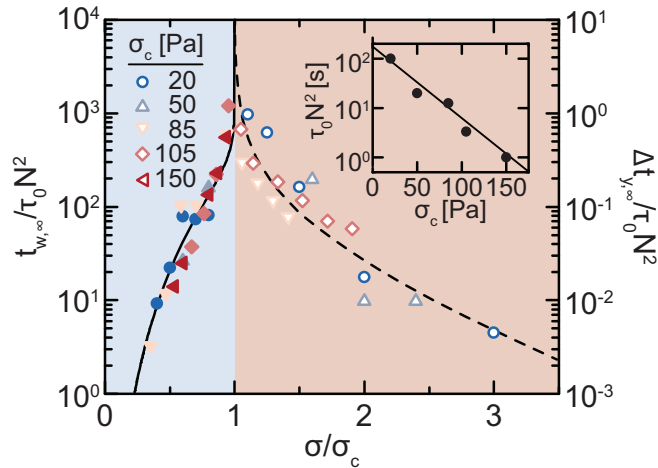
FIG. 4. Normalized waiting time $t_{w,\infty}/\tau_0 N^2$ (closed) after which networks no longer yield and the normalized long-time yield plateau $\Delta t_{y,\infty}/\tau_0 N^2$ (open) as a function of normalized stress σ/σ_c for networks with different critical stresses σ_c, corresponding to $0.013 \leqslant \phi \leqslant 0.027$. Solid and dashed curves are predictions from Eq. (1) and a self-healing active bond rupture model [34], respectively. Inset: Normalization product $\tau_0 N^2$ as a function of σ_c. Solid line is a guide to the eye.

$\tau_0 N^2$. Importantly, this expression correctly captures the divergence of $t_{w,\infty}$ as σ approaches σ_c. These restructuring kinetics contrast strongly with the rapid self-healing dynamics of other yield-stress fluids such as chemically crosslinked polymer networks [29–31] or colloidal gels [32,33] in which the self-healing mechanisms are controlled by the diffusion of molecular crosslinkers and chemical reaction rates.

At higher stresses $\sigma > \sigma_c$, the applied stress is large enough to always yield the sample regardless of t_w. In this regime, yielding dynamics represent a competition between the rate of disentanglement, controlled by the applied stress, and the rate of creation of new entanglements, controlled by fibril dynamics. Because the networks are weaker immediately after yielding, we focus on the magnitude of the yield time $\Delta t_{y,\infty}$ measured after long t_w as representative of an equilibrated sample. For high stress $\sigma \gg \sigma_c$, $\Delta t_{y,\infty}$ exhibits an exponential decay with increasing σ (Fig. 4). As σ approaches σ_c, $\Delta t_{y,\infty}$ diverges because the network can fully support the stress. There are a variety of models [21,35–37] that predict yield time as a function of applied stress for disordered materials. Many of these models assume that the network is formed by bonds that dissociate over time to allow the material to relax. This bond dissociation rate is exponentially enhanced by applied stresses so that the material fails faster at high stresses. The model is agnostic to physicochemical nature of the bond. While the exponential decay of $\Delta t_{y,\infty}$ is observed for CNF networks at large stresses (Fig. 4), the yield time diverges near the σ_c rather than approaching finite value. A recently proposed self-healing activated bond rupture (SH-ABR) model [34,38], however, accounts for this yield time divergence by incorporating the ability of the material to reform entanglements. This SH-ABR model captures the dependence of $\Delta t_{y,\infty}$ on σ across orders of magnitude in time

and accurately predicts the divergence near σ_c and the transition to an exponential decay when $\sigma \gg \sigma_c$ (Fig. 4). Thus, fibrillar networks yield because the rate of chain disentanglement is stress enhanced beyond the rate at which they reform.

Extracellular matrices surrounding animal cells (e.g., collagen) or in plant cell walls [39–41] similarly yield and recover, but the underlying mechanisms contrast with the cellulose model presented in this study. Our cellulose networks yield due to fibril disentanglement but can recover over long timescales with dynamic reconstruction of the entangled networks. Conversely, yielding in collagen and fibrin matrices is typically associated with plastic deformation and rupture of fibril bundles and dissociation of crosslinks [42]. Matrix lengthening also drives collagen fiber realignment and densification, facilitating material recovery via the formation of new crosslinks between adjacent fibers [43,44]. Akin to our cellulose gels following re-entanglement, a matrix with newly formed crosslinks has a configuration that differs from its initial reference state. The kinetics of the CNF re-entanglement, described by the product $\tau_0 N^2$ characterizing the segmental dynamics [24], accelerate in more concentrated suspensions (inset to Fig. 4) similar to behavior observed for peptide hydrogels [45], gelatin networks [46], and colloidal gels [47,48]. We attribute the faster kinetics to the decreasing number of segments N between entanglements in more concentrated gels. These mechanisms suggest that the CNF dynamics control the rate of formation of physical entanglements before and after yielding, in contrast to the mechanisms described for other structural biomacromolecules such as collagen. Although much of this discussion surrounding the physical mechanisms underlying the yielding and recovery processes of CNF gels is specific to semiflexible fibers, the connection between nanoscale dynamics controlling fluid structure, fluid thixotropy, and the yield stress can be generalized to other systems.

In conclusion, we report a bifurcation of the yielding response in soft, amorphous gels made of cellulose nanofibrils. The observed bifurcation separates two mechanical states of the gel—an elastic solid and a viscous fluid—and serves as a robust and unambiguous measurement of the yield stress for a thixotropic material, independent of sample age or shear history. We also demonstrate that the evolution of the yield time in these materials can be well described by the segmental dynamics of the fibrils. From this work, we construct a comprehensive and consistent picture that relates the nanoscale dynamics to the thixotropic yielding response of fibrillar networks. Although descriptions for underlying dynamics will be different for different systems, our results suggest that the bifurcating stress that dictates the yield response of materials serves as a general metric to uniquely identify the yield stress in complex fluids.

[1] P. C. Møller, J. Mewis, and D. Bonn, Yield stress and thixotropy: On the difficulty of measuring yield stresses in practice, Soft Matter **2**, 274 (2006).

[2] M. Dinkgreve, J. Paredes, M. M. Denn, and D. Bonn, On different ways of measuring "the" yield stress, J. Non-Newton. Fluid Mech. **238**, 233 (2016).

[3] G. J. Donley, J. R. de Bruyn, G. H. McKinley, and S. A. Rogers, Time-resolved dynamics of the yielding transition in soft materials, J. Non-Newton. Fluid Mech. **264**, 117 (2019).

[4] A. E. James, D. J. Williams, and P. R. Williams, Direct measurement of static yield properties of cohesive suspensions, Rheol. Acta **26**, 437 (1987).

[5] D. Bonn, M. M. Denn, L. Berthier, T. Divoux, and S. Manneville, Yield stress materials in soft condensed matter, Rev. Mod. Phys. **89**, 035005 (2017).

[6] R. G. Larson and Y. Wei, A review of thixotropy and its rheological modeling, J. Rheol. **63**, 477 (2019).

[7] P. R. de Souza Mendes and R. L. Thompson, Time-dependent yield stress materials, Curr. Opin. Colloid Interface Sci. **43**, 15 (2019).

[8] P. Moller, A. Fall, V. Chikkadi, D. Derks, and D. Bonn, An attempt to categorize yield stress fluid behaviour, Philos. Trans. R. Soc. A Math. Phys. Eng. Sci. **367**, 5139 (2009).

[9] P. Coussot, Q. D. Nguyen, H. T. Huynh, and D. Bonn, Viscosity bifurcation in thixotropic, yielding fluids, J. Rheol. **46**, 573 (2002).

[10] Y. Wei, M. J. Solomon, and R. G. Larson, Letter to the Editor: Modeling the nonmonotonic time-dependence of viscosity bifurcation in thixotropic yield-stress fluids, J. Rheol. **63**, 673 (2019).

[11] O. Nechyporchuk, M. N. Belgacem, and F. Pignon, Current progress in rheology of cellulose nanofibril suspensions, Biomacromolecules **17**, 2311 (2016).

[12] H. N. Xu and Y. H. Li, Decoupling arrest origins in hydrogels of cellulose nanofibrils, ACS Omega **3**, 1564 (2018).

[13] F. C. MacKintosh, J. Käs, and P. A. Janmey, Elasticity of Semiflexible Biopolymer Networks, Phys. Rev. Lett. **75**, 4425 (1995).

[14] M. Pääkkö, M. Ankerfors, H. Kosonen, A. Nykänen, S. Ahola, M. Österberg, J. Ruokolainen, J. Laine, P. T. Larsson, O. Ikkala, and T. Lindström, Enzymatic hydrolysis combined with mechanical shearing and high-pressure homogenization for nanoscale cellulose fibrils and strong gels, Biomacromolecules **8**, 1934 (2007).

[15] N. Quennouz, S. M. Hashmi, H. S. Choi, J. W. Kim, and C. O. Osuji, Rheology of cellulose nanofibrils in the presence of surfactants, Soft Matter **12**, 157 (2016).

[16] R. J. Hill, Elastic modulus of microfibrillar cellulose gels, Biomacromolecules **9**, 2963 (2008).

[17] H. H. Winter and F. Chambon, Analysis of linear viscoelasticity of a crosslinking polymer at the gel point, J. Rheol. **30**, 367 (1986).

[18] H. H. Winter and M. Mours, Rheology of polymers near liquid-solid transitions, Adv. Polym. Sci.Advances in Polymer Science, **134**, 165 (1997).

[19] J.-F. Berret and Y. Séréro, Evidence of Shear-Induced Fluid Fracture in Telechelic Polymer Networks, Phys. Rev. Lett. **87**, 048303 (2001).

[20] T. Chevalier, S. Rodts, X. Chateau, J. Boujlel, M. Maillard, and P. Coussot, Boundary layer (shear-band) in frustrated viscoplastic flows, Europhysics Lett. **102**, 48002 (2013).

[21] P. J. Skrzeszewska, J. Sprakel, F. A. de Wolf, R. Fokkink, M. A. Cohen Stuart, and J. van der Gucht, Fracture and self-healing in a well-defined self-assembled polymer network, Macromolecules **43**, 3542 (2010).

[22] M. Leocmach, C. Perge, T. Divoux, and S. Manneville, Creep and Fracture of a Protein Gel under Stress, Phys. Rev. Lett. **113**, 038303 (2014).

[23] S. P. Meeker, R. T. Bonnecaze, and M. Cloitre, Slip and flow in pastes of soft particles: Direct observation and rheology, J. Rheol. **48**, 1295 (2004).

[24] S. Prager and M. Tirrell, The healing process at polymer-polymer interfaces, J. Chem. Phys. **75**, 5194 (1981).

[25] R. P. Wool, B. L. Yuan, and O. J. McGarel, Welding of polymer interfaces, Polym. Eng. Sci. **29**, 1340 (1989).

[26] P. G. De Gennes, The formation of polymer/polymer junctions, Tribol. Ser. **7**, 355 (1981).

[27] P. Prentice, Influence of molecular weight on the fracture of poly(methyl methacrylate) (PMMA), Polymer **24**, 344 (1983).

[28] A. A. Griffith, The phenomena of rupture and flow in solids, Philos. Trans. R. Soc. A Math. Phys. Eng. Sci. **221**, 163 (1921).

[29] Z. Wei, J. H. Yang, J. Zhou, F. Xu, M. Zrínyi, P. H. Dussault, Y. Osada, and Y. M. Chen, Self-healing gels based on constitutional dynamic chemistry and their potential applications, Chem. Soc. Rev. **43**, 8114 (2014).

[30] S. Basak, J. Nanda, and A. Banerjee, Multi-stimuli responsive self-healing metallo-hydrogels: Tuning of the gel recovery property, Chem. Commun. **50**, 2356 (2014).

[31] Y. Shi, M. Wang, C. Ma, Y. Wang, X. Li, and G. Yu, A conductive self-healing hybrid gel enabled by metal-ligand supramolecule and nanostructured conductive polymer, Nano Lett. **15**, 6276 (2015).

[32] H. Wang, M. B. Hansen, D. W. Löwik, J. C. Van Hest, Y. Li, J. A. Jansen, and S. C. Leeuwenburgh, Oppositely charged Gelatin nanospheres as building blocks for injectable and biodegradable gels, Adv. Mater. **23**, 119 (2011).

[33] M. Diba, H. Wang, T. E. Kodger, S. Parsa, and S. C. G. Leeuwenburgh, Highly elastic and self-healing composite colloidal gels, Adv. Mater. **29**, 1604672 (2017).

[34] S. Mora, The kinetic approach to fracture in transient networks, Soft Matter **7**, 4908 (2011).

[35] S. N. Zhurkov, Kinetic concept of the strength of solids, Int. J. Fract. **26**, 295 (1984).

[36] L. Vanel, S. Ciliberto, P.-P. Cortet, and S. Santucci, Time-dependent rupture and slow crack growth: Elastic and viscoplastic dynamics, J. Phys. D. Appl. Phys. **42**, 214007 (2009).

[37] J. Sprakel, S. B. Lindström, T. E. Kodger, and D. A. Weitz, Stress Enhancement in the Delayed Yielding of Colloidal Gels, Phys. Rev. Lett. **106**, 248303 (2011).

[38] C. Ligoure and S. Mora, Fractures in complex fluids: The case of transient networks, Rheol. Acta **52**, 91 (2013).

[39] D. J. Cosgrove, Loosening of plant cell walls by expansins, Nature **407**, 321 (2000).

[40] D. J. Cosgrove, Plant cell wall extensibility: Connecting plant cell growth with cell wall structure, mechanics, and the action of wall-modifying enzymes, J. Exp. Bot. **67**, 463 (2016).

[41] A. J. Bidhendi and A. Geitmann, Relating the mechanics of the primary plant cell wall to morphogenesis, J. Exp. Bot. **67**, 449 (2016).

[42] N. A. Kurniawan, B. E. Vos, A. Biebricher, G. J. Wuite, E. J. Peterman, and G. H. Koenderink, Fibrin networks support recurring mechanical loads by adapting their structure across multiple scales, Biophys. J. **111**, 1026 (2016).

[43] E. Ban, J. M. Franklin, S. Nam, L. R. Smith, H. Wang, R. G. Wells, O. Chaudhuri, J. T. Liphardt, and V. B. Shenoy, Mechanisms of plastic deformation in collagen networks induced by cellular forces, Biophys. J. **114**, 450 (2018).

[44] E. Ban, H. Wang, J. Matthew Franklin, J. T. Liphardt, P. A. Janmey, and V. B. Shenoy, Strong triaxial coupling and anomalous Poisson effect in collagen networks, Proc. Natl. Acad. Sci. USA **116**, 6790 (2019).

[45] C. Veerman, K. Rajagopal, C. S. Palla, D. J. Pochan, J. P. Schneider, and E. M. Furst, Gelation kinetics of β-hairpin peptide hydrogel networks, Macromolecules **39**, 6608 (2006).

[46] H. B. Bohidar and S. S. Jena, Kinetics of sol-gel transition in thermoreversible gelation of gelatin, J. Chem. Phys. **98**, 8970 (1993).

[47] P. Sandkühler, J. Sefcik, and M. Morbidelli, Kinetics of gel formation in dilute dispersions with strong attractive particle interactions, Adv. Colloid Interface Sci. **108-109**, 133 (2004).

[48] H. Wu, J. J. Xie, and M. Morbidelli, Kinetics of colloidal gelation and scaling of the gelation point, Soft Matter **9**, 4437 (2013).